Vol 464|25 March 2010|doi:10.1038/nature08845

ARTICLES

Neurogenic radial glia in the outer subventricular zone of human neocortex

David V. Hansen[1,2]*, Jan H. Lui[1,2,3]*, Philip R. L. Parker[1,2,4] & Arnold R. Kriegstein[1,2]

Neurons in the developing rodent cortex are generated from radial glial cells that function as neural stem cells. These epithelial cells line the cerebral ventricles and generate intermediate progenitor cells that migrate into the subventricular zone (SVZ) and proliferate to increase neuronal number. The developing human SVZ has a massively expanded outer region (OSVZ) thought to contribute to cortical size and complexity. However, OSVZ progenitor cell types and their contribution to neurogenesis are not well understood. Here we show that large numbers of radial glia-like cells and intermediate progenitor cells populate the human OSVZ. We find that OSVZ radial glia-like cells have a long basal process but, surprisingly, are non-epithelial as they lack contact with the ventricular surface. Using real-time imaging and clonal analysis, we demonstrate that these cells can undergo proliferative divisions and self-renewing asymmetric divisions to generate neuronal progenitor cells that can proliferate further. We also show that inhibition of Notch signalling in OSVZ progenitor cells induces their neuronal differentiation. The establishment of non-ventricular radial glia-like cells may have been a critical evolutionary advance underlying increased cortical size and complexity in the human brain.

One of the most marked evolutionary changes underlying the unique cognitive abilities of humans is the greatly enlarged cerebral cortex. This change must be reflected in differences in progenitor cell number and/or proliferative output during development. There has been considerable progress in understanding progenitor cell behaviour in the developing rodent cortex, where neurogenic cell divisions are confined to a narrow region of proliferative cells near the cerebral ventricles[1]. Cortical neurons arise from radial glial (RG) cells, the epithelial stem cells that line these ventricles[2–4]. RG cells in the ventricular zone (VZ) generate intermediate progenitor cells that migrate into the SVZ and further proliferate to increase neuronal number[5,6].

A distinguishing feature of primate corticogenesis is the appearance of the OSVZ during mid-gestation[7–9]. Cell-labelling studies in primates have shown that cell divisions in both the OSVZ and the VZ coincide with the major wave of cortical neurogenesis, suggesting that OSVZ cells produce neurons[10,11]. However, the progenitor cell types in the OSVZ and the extent to which they participate in neurogenesis have not been characterized. Furthermore, unique features of human cortical development probably underlie neurodevelopmental disorders that affect the cerebral cortex, such as autism and schizophrenia. Here we describe classes of radial glia-like cells and transit-amplifying cells in the human OSVZ that contribute significantly to neurogenesis. OSVZ radial glia-like cells show unusual cell cycle behaviours that further distinguish them from traditional RG cells. These results indicate a new mechanism for cortical expansion outside the ventricular epithelium through the addition of radial columns arising from the OSVZ.

Radial glia-like cells populate the OSVZ

Recent reports have shown that cells expressing the transcription factor PAX6 are found in the OSVZ of human and primate cortex[9,12,13], unlike the rodent where PAX6 is expressed mainly by RG cells in the VZ[14]. It has been suggested that PAX6$^+$ cells in the OSVZ include both progenitor cells and postmitotic neurons[9,13]. We examined sections of fetal cortex and found that most PAX6$^+$ cells (>90%) in the human OSVZ co-expressed the neural stem/progenitor cell marker SOX2, and many also expressed the proliferation marker Ki67 (Supplementary Fig. 1), indicating that most of them are progenitor cells. We sought to characterize the progenitor cells in the human OSVZ further, and determine whether any are RG cells.

RG cells are characterized, in part, by their distinctive morphology, with an apical process extending to the ventricle and a basal process extending to the pia that can guide radial neuronal migration. We examined whether the morphology of OSVZ cells resembled RG cells by focally electroporating dye-conjugated dextran[15] in the OSVZ to label cells. We routinely observed OSVZ cells that resembled RG cells by having a long radial process. However, these cells showed only basal and not apical processes (Supplementary Fig. 2). For example, a single electroporation labelled five OSVZ cells that all demonstrated basal but not apical processes. These cells all expressed SOX2, further resembling RG cells (Fig. 1a).

To address whether OSVZ RG-like cells were actively cycling, we infected cortical fragments from gestational week 14 (GW14) with green fluorescent protein (GFP)-retrovirus to label dividing cells, and cultured tissue slices. Many GFP-labelled OSVZ cells had long basal but not apical processes and expressed PAX6 and SOX2 (Fig. 1b). To quantify the number of progenitor cells with this morphology, we stained for phospho-vimentin, which marks the cytoplasm of neural progenitors in and directly after M-phase of the cell cycle. About half of the SOX2$^+$ phospho-vimentin$^+$ cells in the OSVZ showed a clear basal but no apical process (141 out of 304, GW15.5), often with varicosities similar to M-phase RG cells (also see Fig. 1c, GW17)[3,16]. Phospho-vimentin$^+$ cells with this morphology nearly always expressed the RG markers SOX2 (267 out of 272), PAX6 (27 out of 27), nestin (31 out of 31) and GFAP (20 out of 20), but never the early neuronal markers DCX (27 out of 27) or βIII-tubulin (22 out of 22) (Supplementary Fig. 3). On the basis of the number of phospho-vimentin$^+$ cells with basal fibres in the OSVZ (145 out of 367) and

[1]Eli and Edythe Broad Center of Regeneration Medicine and Stem Cell Research, [2]Department of Neurology, [3]Biomedical Sciences Graduate Program, [4]Neuroscience Graduate Program, University of California San Francisco, 513 Parnassus Avenue, San Francisco, California 94143, USA.
*These authors contributed equally to this work.

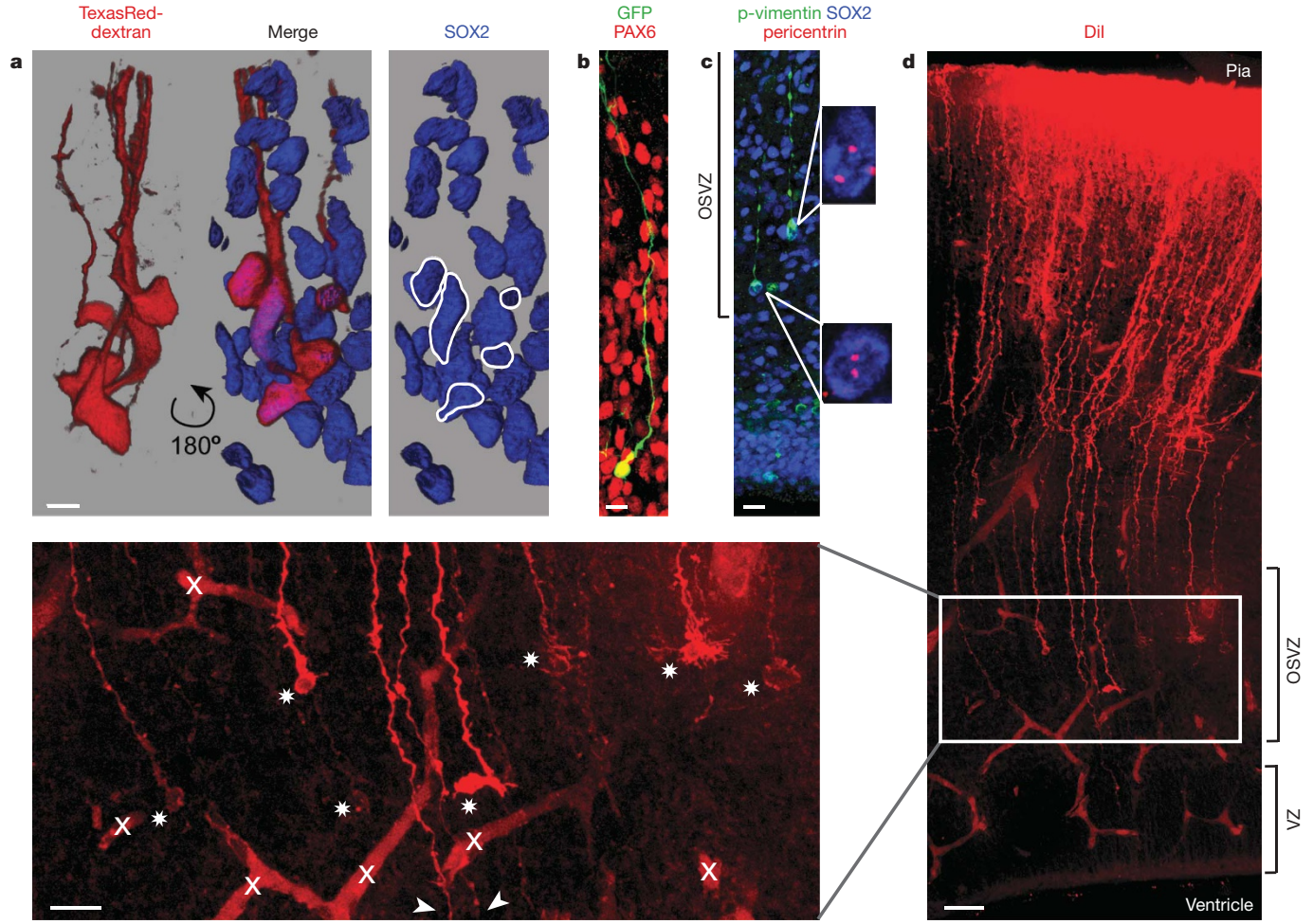

Figure 1 | The human OSVZ is populated with non-epithelial radial glia-like cells. a, Five OSVZ cells in GW15.5 cortex labelled by focal dye electroporation followed by immunostaining for SOX2 (blue). Cell bodies were labelled 100 μm from injection site through their basal processes. Three-dimensional rendering is shown. Nuclei are outlined in white. Scale bar, 5 μm. **b**, Representative GFP-retrovirus-labelled cell co-expressing PAX6 (red) in GW14 OSVZ. Scale bar, 15 μm. **c**, GW17 cortex stained for SOX2 (blue), phospho-vimentin (p-vimentin; green, cytoplasm of M-phase cells), and pericentrin (red, centrosomes), demonstrating morphology and centrosome location of SOX2$^+$ OSVZ cells during mitosis. Scale bar, 15 μm. **d**, Fixed GW15 cortex labelled pially with DiI-coated beads (DiOlistics). Inset demonstrates dye diffusion along radial processes from the pia terminating at distinct cell bodies in the OSVZ (stars) amid coexistent radial fibres that traverse the OSVZ to the ventricle (arrowheads) and autofluorescent blood vessels ('x'). Scale bars, 40 μm (**d**) and 20 μm (inset).

the strong correlation of these cells with RG markers, we estimate that about 40% of all OSVZ progenitors are RG-like cells.

The radial processes of RG cells in the VZ support neuronal migration and underlie the columnar architecture of the cortex[17,18]. The basal processes of OSVZ cells could serve a similar function, particularly if they extend to the pia. We applied DiI-coated beads to the pial surface of fixed cortical tissue (DiOlistics[19]) to label radial fibres and their corresponding cell bodies. Many OSVZ cells were seen with RG-like morphology but lacking apical processes (Fig. 1d), showing that at least a subset of OSVZ cells contacts the pia. By contrast, ventricular labelling showed only rare OSVZ cells labelled through their apical processes (Supplementary Fig. 4).

To rule out that OSVZ RG-like cells have ventricular processes that escaped labelling with other methods, we examined the ventricular surface to look for evidence of apical endings of OSVZ cells. The centrosomes of OSVZ progenitors reside in the OSVZ where the cells undergo mitosis (Fig. 1c). In contrast, the centrosomes of RG cells in the VZ are anchored at the ventricular surface, to which VZ cell bodies migrate to undergo mitosis (Supplementary Fig. 5a)[20]. We stained the ventricular surface of whole-mount tissue sections to examine the presence of centrosomes within the array of RG cell endfeet. An 'en face' view showed that most endfeet (>94%) contained centrosomes and thus originated from ventricular RG cells, confirming that most OSVZ cells do not contact the ventricle (Supplementary Fig. 5b).

Together, these results show that the human OSVZ contains a new class of actively dividing, non-epithelial progenitors that can maintain contact with the pia but not the ventricle. Owing to their radial morphology and expression of nuclear and cytoplasmic markers characteristic of RG cells, we will refer to these cells as oRG (OSVZ radial glia-like) cells to set them apart from traditional RG cells in the ventricular epithelium (vRG cells).

oRG cells self-renew and produce intermediate progenitor cells

An important feature of vRG cells is their ability to undergo several self-renewing divisions. To determine whether oRG cells also do this, we used GFP-expressing adenovirus (adenoGFP) to label cells in cultured slices where the VZ and inner SVZ (ISVZ) had been removed by microdissection, and then sequentially treated with the thymidine analogues BrdU (5-bromodeoxyuridine) and EdU (5-ethynyldeoxyuridine) spaced 36 h apart. This excluded VZ–ISVZ progenitors from the analysis and tested whether OSVZ progenitors go through S-phase more than once. We searched for GFP$^+$ cells with oRG morphology and analysed them for BrdU and EdU labelling. More than half (13 out of 21) were double-labelled, and 6 out of 21 were single-labelled (Fig. 2a). This suggested that oRG cells could divide and self-renew.

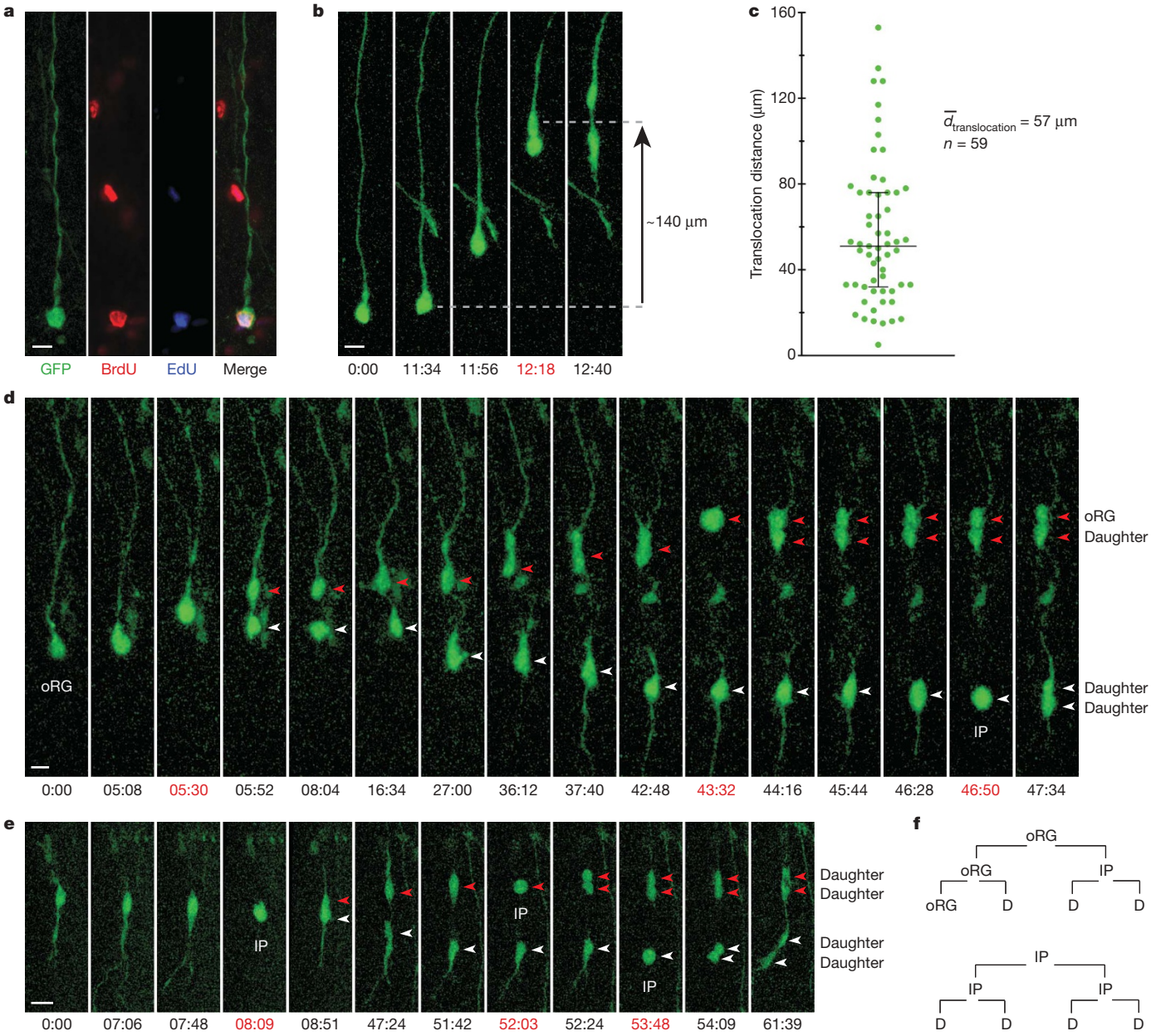

Figure 2 | oRG cells self-renew and produce intermediate progenitor daughter cells. **a**, AdenoGFP-labelled oRG cell in OSVZ slice culture (GW15), sequentially treated with the thymidine analogues BrdU (red) and EdU (blue) spaced 36 h apart to label cells that passed through S-phase twice (see text for cell counts). Scale bar, 10 μm. **b**, oRG cell undergoes 'mitotic somal translocation' directly before cell division. An adenoGFP-labelled GW15 cortical slice was imaged at 22-min intervals beginning 26 h after infection (see Supplementary Movie 2). Times, h:min (red for mitosis) (for **b**, **d** and **e**). Scale bar, 15 μm. **c**, Quantification of mitotic somal translocation distances of oRG cell divisions from GW15 time-lapse sequences. The median and interquartile range are shown. $n = 59$; mean distance = 57 μm. **d**, oRG cell undergoes two self-renewing divisions followed by division of the initial daughter cell (intermediate progenitor, IP). GW15 cortical slice was imaged as in **b** beginning 40 h after infection (see Supplementary Movie 4). Red and white arrowheads follow the lineages of oRG cell and oRG daughter, respectively. Scale bar, 10 μm. **e**, Bipolar intermediate progenitor cell resembling an oRG daughter undergoes two rounds of proliferative division. Imaging began 42 h after infection at 21-min intervals. Red and white arrowheads follow the lineages of the two intermediate progenitor daughters. Scale bar, 20 μm. **f**, Lineage relationships between cells in **d** and **e**. oRG cells can divide asymmetrically to self-renew and generate an intermediate progenitor cell. Intermediate progenitor cells can also undergo multiple divisions. D, daughter.

We used real-time imaging to observe the behaviours of oRG cells and their daughters. AdenoGFP-labelled oRG cells frequently divided and exhibited a surprising behaviour where the cell soma moved rapidly up the basal fibre before cytokinesis (Fig. 2b and Supplementary Movies 1 and 2). We term this behaviour 'mitotic somal translocation'. The duration of translocation was usually <60 min, with distances averaging 57 μm and sometimes exceeding 100 μm (Fig. 2b, c). Of the hundreds of oRG cell divisions observed, all but three divided with a horizontal cleavage plane with the upper daughter inheriting the basal fibre and maintaining oRG morphology, consistent with asymmetric self-renewing divisions. The lower oRG daughter usually became radially bipolar, with the more prominent process directed towards the ventricle. The mitotic somal translocation of oRG cells contrasts with the interkinetic nuclear migration of RG and neuroepithelial cells, in which the nucleus moves towards the ventricle before mitosis.

We imaged for longer periods and observed oRG cells dividing twice, with two distinct translocations and the upper cell inheriting the radial fibre (Supplementary Movie 3). We also routinely observed the lower daughter of an oRG cell divide again, showing that oRG daughters can also be progenitors (Fig. 2d and Supplementary Movies 2 and 4). Limitations in slice culture viability made it difficult to observe cells

for more than two divisions. However, we observed cells resembling bipolar oRG daughters (similar to Fig. 2d at time 37 h 40 min, white arrowhead) that divided twice (Fig. 2e), suggesting that oRG daughters can undergo transit-amplifying divisions. Together, these results support a model in which the OSVZ contains at least two different types of progenitors that can divide multiple times (Fig. 2f).

oRG cells are neurogenic

To test whether OSVZ progenitor cells produce neurons, we dissected OSVZ tissue away from the VZ–ISVZ and cultured dissociated cells with BrdU to label newborn cells. BrdU$^+$ βIII-tubulin$^+$ neurons were present in the VZ–ISVZ and OSVZ but not cortical plate cultures (Supplementary Fig. 6a). About 5% of βIII-tubulin$^+$ neurons from OSVZ cultures (60 out of 1,295) were BrdU$^+$, indicating that OSVZ progenitor cells produced neurons. It has been reported that two-thirds of GABA (γ-aminobutyric acid)-containing inhibitory neurons in the human cortex are generated locally[21]. We therefore looked for GABA$^+$ BrdU$^+$ neurons in our VZ–ISVZ and OSVZ cultures. Of the neurons from OSVZ cultures that were GABA$^+$ (82 out of 1,295), not one was BrdU$^+$ (Supplementary Fig. 6b). Cultured VZ–ISVZ cells gave similar results, suggesting that cortical progenitors do not produce inhibitory neurons. Alternatively, our culture conditions may not support their production. In contrast, some cultured cells expressed TBR2 (also known as EOMES), a transcription factor expressed by intermediate progenitor cells and newly born neurons of the excitatory lineage[22–24]. Nearly all of these (63 out of 65 in OSVZ culture) were BrdU$^+$ and thus must have originated from SOX2$^+$ or TBR2$^+$ cells, and many of these (25 out of 63) were also βIII-tubulin$^+$, suggesting that excitatory neurons were being generated in the human OSVZ (Supplementary Fig. 6b).

These results indicated that neurons are produced by OSVZ progenitor cells but did not identify the cell type of origin. To explore whether oRG cells produce neurons, we monitored oRG cell divisions in real time and determined daughter cell fate by immunostaining. Early commitment to a neuronal lineage was indicated by the expression of TBR2 or ASCL1 (a transcription factor reported to specify GABAergic neuron fate in primate cortical progenitors[21,25]). Most of the oRG cell divisions analysed (13 out of 17) showed that both daughters continued to express SOX2 but not TBR2 or ASCL1, even after another division (Fig. 3a and Supplementary Fig. 7). Occasionally, the non-oRG daughter even extended a basal process and re-acquired oRG cell morphology (Supplementary Fig. 8). This supports a model of cortical neurogenesis in which oRG cells produce daughter cells that often proliferate before differentiation, thus expanding the OSVZ progenitor pool.

We observed six OSVZ cell divisions that gave rise to TBR2$^+$ daughters, three of which originated from progenitors with oRG morphology (Fig. 3b and Supplementary Fig. 9). In each case, the cell that inherited the basal process remained SOX2$^+$ TBR2$^-$, whereas the daughter cell became TBR2$^+$ and in two of three cases divided again. These examples are evidence of asymmetric oRG cell divisions that yield a self-renewed oRG cell and a neuronally committed intermediate progenitor cell. Of the four divisions we observed that gave rise to ASCL1$^+$ cells, one was from a progenitor with oRG morphology (Fig. 3c). The oRG cell retained the basal process and expressed only SOX2—a further example of self-renewing, neurogenic oRG cell division.

Our observation that oRG cells can directly produce either TBR2$^+$ or ASCL1$^+$ cells suggested that oRG cells generate neuronal precursors for both excitatory and inhibitory lineages. To determine the relative amounts of these two precursor types, we stained cryosections for TBR2 and ASCL1 along with SOX2. Surprisingly, all ASCL1$^+$ cells co-expressed SOX2 and/or TBR2 (Supplementary Fig. 10), placing cortical ASCL1$^+$ progenitors in the same lineage as TBR2$^+$ cells. We were therefore unable to distinguish distinct precursors for inhibitory neurons because they seem to share a common precursor with

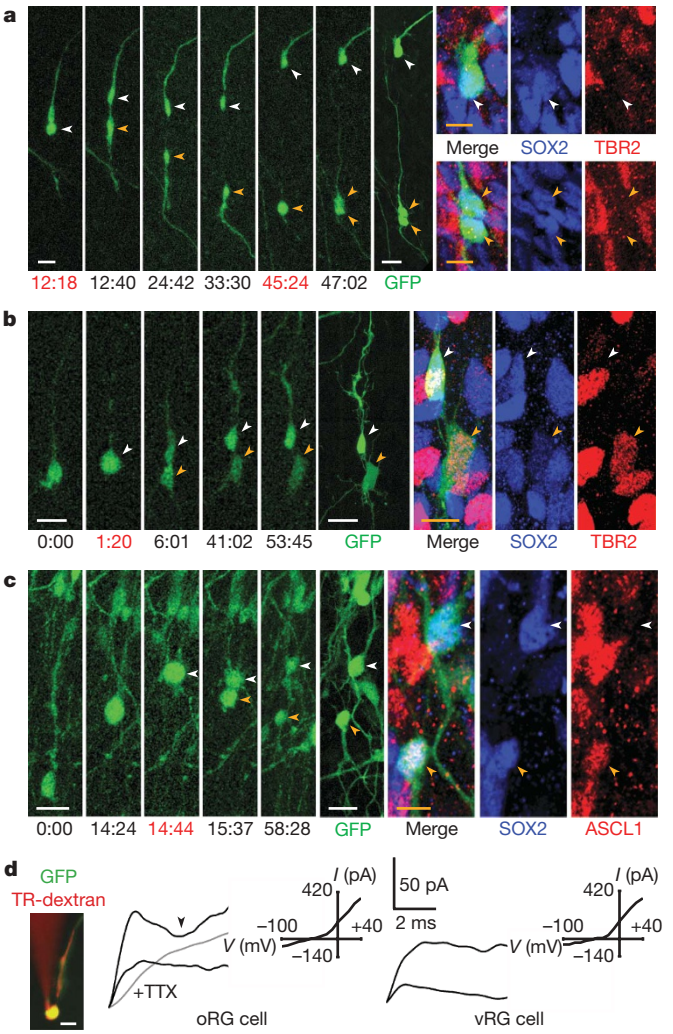

Figure 3 | Daughters of oRG cells are neuronal progenitors. a, Proliferative division of oRG daughter expands progenitor cell number. An adenoGFP-labelled cortical slice was imaged at 22-min intervals (continuation of Fig. 2b), followed by immunostaining to analyse daughter cell fates. Self-renewed oRG cell (white arrowhead) and intermediate progenitor daughter cells (yellow arrowheads) remain undifferentiated (SOX2$^+$ TBR2$^-$). **b**, Asymmetric oRG cell division produces a self-renewed oRG cell (SOX2$^+$ TBR2$^-$, white arrowhead) and a multipolar TBR2$^+$ cell (yellow arrowhead). An adenoGFP-labelled cortical slice (GW15.5) was imaged at 20-min intervals, followed by immunostaining. First image shown (t = 0:00) was 91 h after infection. **c**, Asymmetric oRG cell division produces a self-renewed oRG cell (SOX2$^+$ ASCL1$^-$, white arrowhead) and an ASCL1$^+$ daughter (yellow arrowhead), indicative of neuronal commitment. First image shown (t = 0:00) was 87 h after infection. Times, h:min (red for mitoses). Scale bars (**a**–**c**), 20 μm (white) and 10 μm (yellow). **d**, Patch-clamp recordings of representative oRG (adenoGFP and TexasRed (TR)-dextran overlay) and vRG cells. Current–voltage relationships and current traces for voltage steps from −60 mV to −40 mV (bottom black) or −10 mV (top black) are shown. A voltage-sensitive inward current (arrowhead) in the oRG cell is abolished by TTX (grey trace, −10 mV). Scale bar, 10 μm.

excitatory cells. The identification of new markers may help identify subtypes of precursor cells committed to these lineages.

We also examined the membrane properties of oRG cells and compared them to other glial and neuronal cells. In patch-clamp recordings, the input resistances of vRG and oRG cells were comparable (vRG = 557.0 ± 190.4 MΩ (mean ± standard error), n = 3; oRG = 515.4 ± 10.7 MΩ, n = 3), both of which were lower than other OSVZ cells (multipolar = 1,265 ± 217.1 MΩ, bipolar = 1,952.8 ± 357.0 MΩ). However, although vRG cells showed typical passive membrane properties upon depolarization, oRG cells that were seen dividing in time-lapse images showed small, brief, inward, tetrodotoxin

(TTX)-sensitive currents (77.9 ± 34.2 pA; Fig. 3d), suggesting mediation by voltage-gated sodium channels. These currents were also seen in oRG cells patched blindly in acute slices ($n = 3$). Two cells from a symmetrical division of an oRG daughter intermediate progenitor cell also showed similar inward currents that were abolished by TTX (Supplementary Fig. 11). Most multipolar ($n = 4$ of 7) and bipolar ($n = 3$ of 4) cells in the OSVZ also showed fast inward sodium currents (multipolar = 101.4 ± 20.5 pA, bipolar = 60.6 ± 11.1 pA), which were small compared with that of a cortical plate neuron (935.7 pA). A survey of active membrane conductances of OSVZ cells and neurons suggested that these small currents could represent early instances of sodium current underlying action potential firing. In all, the emerging active properties of OSVZ cells are consistent with a neuronal lineage.

OSVZ progenitors outnumber VZ–ISVZ progenitors

A similar lineal relationship exists between RG and intermediate progenitor cells in the OSVZ as in the VZ–ISVZ, but it is unclear how proliferation in these two regions compares throughout

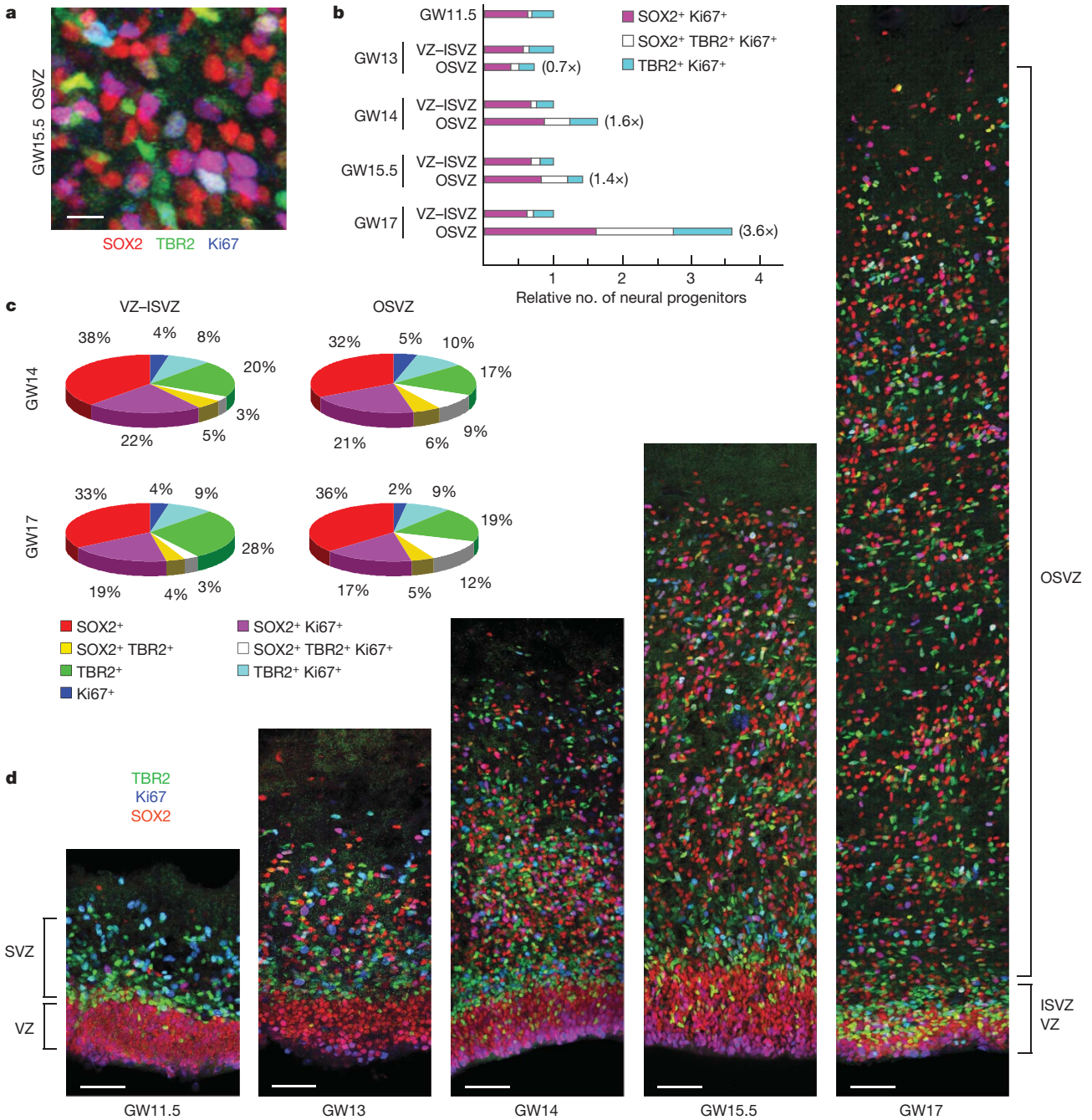

Figure 4 | The human OSVZ is the predominant neurogenic zone during mid-gestational cortical development. **a**, Image of GW15.5 OSVZ demonstrating the extent of SOX2 (red), TBR2 (green) and Ki67 (blue) co-labelling. Scale bar, 10 μm. **b**, Number of actively cycling OSVZ neural progenitors surpasses the VZ–ISVZ during mid-gestation. Ki67$^+$ cells that co-express SOX2 and/or TBR2 were counted and compared over the same width of OSVZ versus VZ–ISVZ in three representative fields for each age (similar to those in **d**), and averaged. **c**, The OSVZ and VZ–ISVZ contain similar proportions of neural progenitor cell types. Cortical progenitors were counted and classified into seven categories on the basis of SOX2, TBR2 and Ki67 expression. See Supplementary Fig. 13 for graphs of all ages. Only progenitor cells were considered, because roughly half of the OSVZ nuclei (marked by 4′,6-diamidino-2-phenylindole (DAPI), not shown) are SOX2$^-$ TBR2$^-$ Ki67$^-$. **d**, Substantial growth of the OSVZ from GW11.5–17 shown by SOX2, TBR2 and Ki67 staining. Progenitor cells in the inner fibre layer (not labelled) were included in OSVZ counts as they are superficial to the VZ–ISVZ. Scale bars, 50 μm.

human cortical development. Before the OSVZ arises, the periventricular region contains vRG cells and intermediate progenitor cells (Fig. 4d, GW11.5) and resembles the developing rodent cortex (compare mouse embryonic day (E)13, Supplementary Fig. 12). By GW13, an increase in SVZ SOX2$^+$ cells marks the development of the OSVZ, which expands massively in the following gestational month (Fig. 4d). In contrast, the VZ–ISVZ remains fairly constant through GW15.5 and diminishes by GW17, suggesting that the OSVZ becomes the predominant proliferative zone.

We compared Ki67-labelling in the OSVZ versus VZ–ISVZ to quantify actively cycling cells over time (Fig. 4b). At GW13, the OSVZ already accounted for >40% of proliferating cells. This increased to ~60% at GW14 and GW15.5, and >75% by GW17, highlighting the extensive contribution of oRG and intermediate progenitor cells in the OSVZ to human corticogenesis. Using SOX2, TBR2 and Ki67 expression to classify cortical progenitors (see Fig. 4a) showed similar proportions of progenitor cell types between the VZ–ISVZ and OSVZ (Fig. 4c and Supplementary Fig. 13). Thus, the human OSVZ is a duplicated neurogenic zone, similar to the VZ–ISVZ in progenitor cell types and proportions but much greater in size.

Finally, we correlated the SOX2 and TBR2 expression profile of OSVZ progenitors with their morphology by staining for phospho-vimentin (data not shown). Almost all phospho-vimentin$^+$ cells with oRG morphology were SOX2$^+$ TBR2$^-$ (65 out of 70), supporting the idea that oRG cells are undifferentiated progenitors. Notably, one-third of phospho-vimentin$^+$ OSVZ cells without oRG morphology were also SOX2$^+$ TBR2$^-$ (29 out of 81). Thus, cells with oRG morphology account for only a subset of undifferentiated OSVZ progenitors (65 oRGs out of 94 total SOX2$^+$ TBR2$^-$ cells). This corroborates our real-time imaging and fate analysis of oRG cell divisions, in

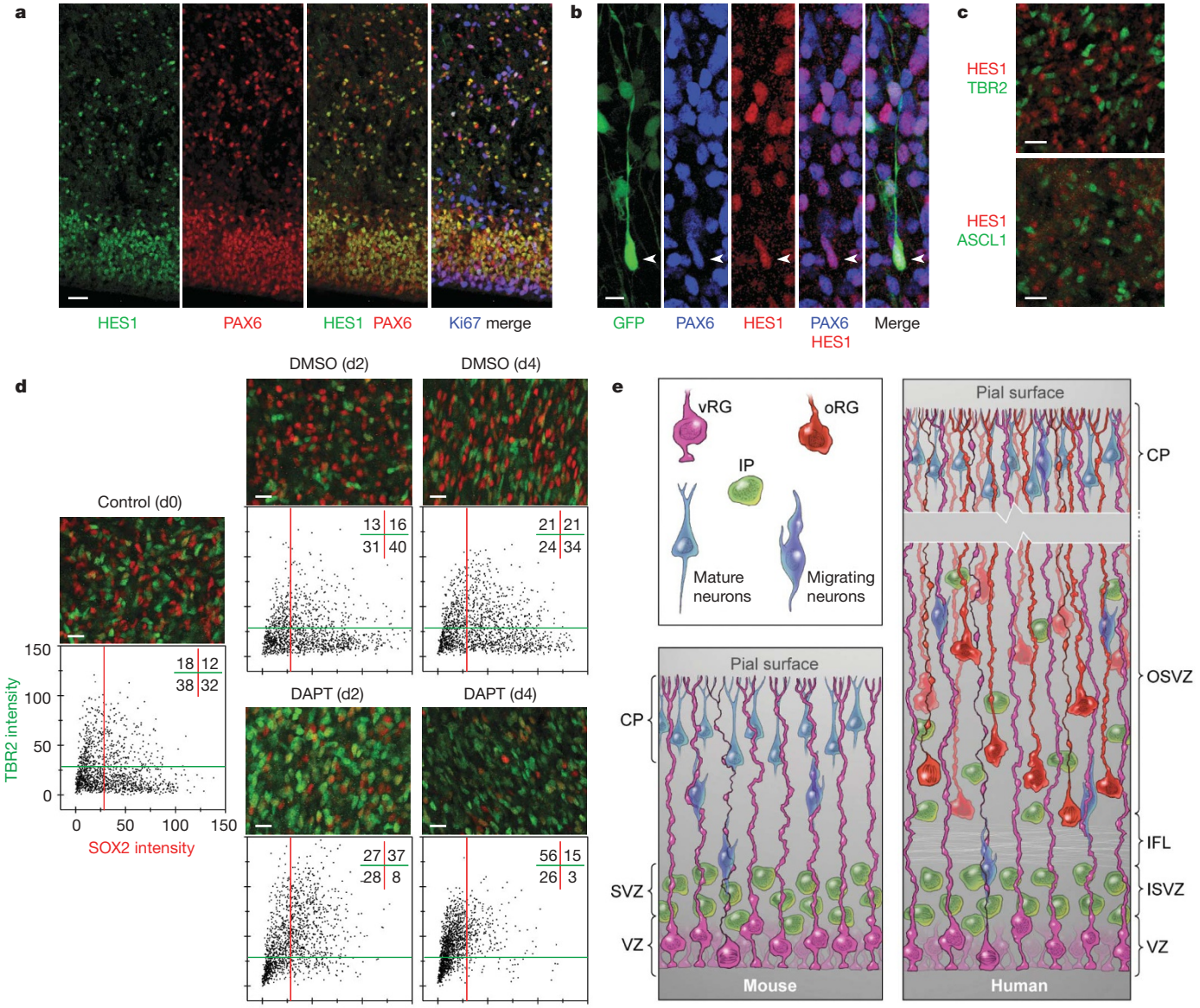

Figure 5 | OSVZ progenitors require Notch signalling to remain undifferentiated. **a**, Co-expression analysis of the Notch effector HES1 (green), PAX6 (red) and Ki67 (blue) in GW15.5 cryosection. Scale bar, 25 μm. **b**, AdenoGFP-labelled oRG cell (white arrowhead) expressing PAX6 (blue) and HES1 (red) in a GW15.5 cortical slice (see text for cell counts). Scale bar, 10 μm. **c**, The Notch effector HES1 (red) does not co-label with markers of neuronal commitment (TBR2 or ASCL1, green) in GW15.5 OSVZ. Scale bars, 20 μm. **d**, OSVZ cells undergo neuronal differentiation after inhibition of Notch signalling. GW15.5 slices cultured with dimethylsulphoxide (DMSO; control) or 10 μM DAPT to inhibit Notch signalling were stained for SOX2 (red) and TBR2 (green) to identify primary versus committed progenitors. Fluorescence intensity of SOX2 versus TBR2 in OSVZ cell nuclei was quantified, plotted, and defined into quadrants using day 0 (d0) as a reference for positive and negative cells. The percentages in each quadrant are shown in the top right. Day 4 percentages are averages of two experiments. Scale bars, 20 μm. **e**, Model of human cortical development in comparison to the mouse. A second set of primary and secondary neural progenitors proliferates extensively in the human OSVZ in addition to periventricular progenitors. CP, cortical plate; IFL, inner fibre layer.

which oRG daughter cells often remained undifferentiated during the ensuing cell division, and underscores the proliferative capacity of OSVZ progenitors.

Notch inhibition induces OSVZ differentiation

It is widely believed that vRG cells must retain certain epithelial properties to maintain progenitor cell status[9,26]. oRG cells are removed from the VZ epithelium and lack apical processes, raising the question of how they persist as RG-like progenitors. A known mechanism of RG cell maintenance is the Notch pathway[27,28]. We therefore investigated whether Notch signalling maintains oRG cell identity.

The Notch effector HES1 was expressed almost exclusively in $PAX6^+$ cells (355 out of 356 OSVZ $HES1^+$ cells were $PAX6^+$) (Fig. 5a). In cultured slices, about 80% (45 out of 56) of adenoGFP-labelled $PAX6^+$ $SOX2^+$ cells with oRG morphology also expressed HES1 (Fig. 5b), supporting a role for Notch in oRG cells. Furthermore, more than half of $PAX6^+$ $SOX2^+$ cells without oRG morphology were also $HES1^+$ (98 out of 158), consistent with our observation that some oRG daughter cells continue to proliferate before differentiation. This suggests that Notch signalling contributes to the expansion of the undifferentiated OSVZ progenitor pool.

Although some $SOX2^+$ cells express TBR2 and/or ASCL1, we saw no co-expression of HES1 with either TBR2 or ASCL1 (Fig. 5c), suggesting that Notch restrains neuronal differentiation. To test the requirement for Notch signalling in OSVZ progenitor cell maintenance, we treated slice cultures with DAPT, a chemical inhibitor of Notch activity. Control slices maintained robust SOX2 expression in the OSVZ and stable ratios of $SOX2^+$, $SOX2^+$ $TBR2^+$, and $TBR2^+$ cells. In contrast, DAPT-treated slices demonstrated an increase in $TBR2^+$ and decrease in $SOX2^+$ cells over time (Fig. 5d). Analysing ASCL1 expression showed similar trends (Supplementary Fig. 14). That $SOX2^+$ cells undergo widespread neuronal differentiation after Notch inhibition shows their overall neurogenic capacity and further underscores the contribution of OSVZ progenitors to human corticogenesis.

Discussion

An expansion of cortical progenitor cell number during evolution must have contributed to the increase in size of the human brain[29]. However, it has been unclear whether expansion of cortical progenitor number is specific to stem versus transit-amplifying cell types—both of which could shape the eventual cellular composition of the cerebral cortex. Our results show that progenitor cells with markers and morphology of neural stem and transit-amplifying cells (RG cells and intermediate progenitor cells) are well represented in the human cortex in both the periventricular zone and the OSVZ. Proliferating cells in the OSVZ were observed decades ago, but the types of cells produced were unknown[30]. Cells in the OSVZ resembling radial glia had also been observed, but their role in cortical development was not defined[31–33]. We have shown that oRG cells, although distinct from the ventricular epithelium, can self-renew and produce neuronal precursors. They further resemble traditional RG cells in terms of marker expression and dependence on Notch signalling. The production of neurons by oRG cells and their daughters presents a more complex scheme of human neurogenesis (Fig. 5e). Although the origin of this previously unappreciated cell type remains unknown, we infer that oRG cells originate in the VZ and use mitotic somal translocation to migrate away. The stepwise translocation of oRG cells towards the cortical plate in coordination with cell divisions helps explain how the OSVZ expands while accumulating large numbers of oRG and intermediate progenitor cells.

Our finding that OSVZ progenitors undergo expansive proliferative divisions contrasts with observations of the rodent SVZ—in which intermediate progenitor cells usually divide only once—and provides a new cellular basis for understanding the evolutionary expansion of surface area in human cortex[34]. It will be interesting to study whether the OSVZ and oRG cells are a general feature of gyrencephalic brain development, especially in non-primate species such as ferret and cat.

The radial unit hypothesis posits that the output of proliferative units (at the ventricle) is translated by glial guides to the expanded cortex in the form of ontogenetic columns[18]. Our results add a layer of complexity to the radial unit model and show that the production of neurons in human cortex occurs simultaneously from primary and secondary progenitor cells in both periventricular and outer subventricular regions—therefore defining two distinct origins for neurons in the mature cortex. Our model suggests that ontogenetic columns can arise from both ventricular and non-ventricular sites during human cortical development. An intriguing future question is whether there are functional differences between neurons generated from these two regions, a feature that would further increase cortical complexity.

METHODS SUMMARY

Fetal cortical tissue was collected from elective pregnancy termination specimens at San Francisco General Hospital, usually within 2 h of the procedure. Tissues were examined only with previous patient consent and in strict observance of legal and institutional ethical regulations. Research protocols were approved by the Committee on Human Research (institutional review board) at University of California, San Francisco. Immunohistochemistry was performed on paraformaldehyde (PFA)-fixed tissue using standard protocols. Dye electroporation was performed on vibratome sections as described[15]. DiOlistics[19] was performed on fixed tissue using fixable CM-DiI (Molecular Probes). Whole-cell patch-clamp electrophysiology was performed using standard protocols. Cortical slice culture was performed as described[6], with some modifications, using GFP-retrovirus or -adenovirus to label cells. Time-lapse and still confocal imaging was performed using a TCS SP5 confocal microscope (Leica). Image analysis, three-dimensional rendering, and cell counting were done in Imaris (Bitplane) and Photoshop (Adobe). Co-localization was calculated using Matlab (Mathworks) and ImarisXT (Bitplane).

Full Methods and any associated references are available in the online version of the paper at www.nature.com/nature.

Received 24 November 2009; accepted 21 January 2010.
Published online 14 February; corrected 25 March 2010 (see full-text HTML version for details).

1. Smart, I. H. Proliferative characteristics of the ependymal layer during the early development of the mouse neocortex: a pilot study based on recording the number, location and plane of cleavage of mitotic figures. *J. Anat.* **116,** 67–91 (1973).
2. Malatesta, P., Hartfuss, E. & Gotz, M. Isolation of radial glial cells by fluorescent-activated cell sorting reveals a neuronal lineage. *Development* **127,** 5253–5263 (2000).
3. Miyata, T., Kawaguchi, A., Okano, H. & Ogawa, M. Asymmetric inheritance of radial glial fibers by cortical neurons. *Neuron* **31,** 727–741 (2001).
4. Noctor, S. C., Flint, A. C., Weissman, T. A., Dammerman, R. S. & Kriegstein, A. R. Neurons derived from radial glial cells establish radial units in neocortex. *Nature* **409,** 714–720 (2001).
5. Haubensak, W., Attardo, A., Denk, W. & Huttner, W. B. Neurons arise in the basal neuroepithelium of the early mammalian telencephalon: a major site of neurogenesis. *Proc. Natl Acad. Sci. USA* **101,** 3196–3201 (2004).
6. Noctor, S. C., Martinez-Cerdeno, V., Ivic, L. & Kriegstein, A. R. Cortical neurons arise in symmetric and asymmetric division zones and migrate through specific phases. *Nature Neurosci.* **7,** 136–144 (2004).
7. Smart, I. H., Dehay, C., Giroud, P., Berland, M. & Kennedy, H. Unique morphological features of the proliferative zones and postmitotic compartments of the neural epithelium giving rise to striate and extrastriate cortex in the monkey. *Cereb. Cortex* **12,** 37–53 (2002).
8. Zecevic, N., Chen, Y. & Filipovic, R. Contributions of cortical subventricular zone to the development of the human cerebral cortex. *J. Comp. Neurol.* **491,** 109–122 (2005).
9. Fish, J. L., Dehay, C., Kennedy, H. & Huttner, W. B. Making bigger brains-the evolution of neural-progenitor-cell division. *J. Cell Sci.* **121,** 2783–2793 (2008).
10. Rakic, P. Neurons in rhesus monkey visual cortex: systematic relation between time of origin and eventual disposition. *Science* **183,** 425–427 (1974).
11. Lukaszewicz, A. *et al.* G1 phase regulation, area-specific cell cycle control, and cytoarchitectonics in the primate cortex. *Neuron* **47,** 353–364 (2005).
12. Bayatti, N. *et al.* A molecular neuroanatomical study of the developing human neocortex from 8 to 17 postconceptional weeks revealing the early differentiation of the subplate and subventricular zone. *Cereb. Cortex* **18,** 1536–1548 (2008).

13. Mo, Z. & Zecevic, N. Is Pax6 critical for neurogenesis in the human fetal brain? *Cereb. Cortex* **18,** 1455–1465 (2008).
14. Götz, M., Stoykova, A. & Gruss, P. Pax6 controls radial glia differentiation in the cerebral cortex. *Neuron* **21,** 1031–1044 (1998).
15. Haas, K., Sin, W. C., Javaherian, A., Li, Z. & Cline, H. T. Single-cell electroporation for gene transfer *in vivo*. *Neuron* **29,** 583–591 (2001).
16. Weissman, T., Noctor, S. C., Clinton, B. K., Honig, L. S. & Kriegstein, A. R. Neurogenic radial glial cells in reptile, rodent and human: from mitosis to migration. *Cereb. Cortex* **13,** 550–559 (2003).
17. Rakic, P. Developmental and evolutionary adaptations of cortical radial glia. *Cereb. Cortex* **13,** 541–549 (2003).
18. Rakic, P. Specification of cerebral cortical areas. *Science* **241,** 170–176 (1988).
19. Gan, W. B., Grutzendler, J., Wong, W. T., Wong, R. O. & Lichtman, J. W. Multicolor "DiOlistic" labeling of the nervous system using lipophilic dye combinations. *Neuron* **27,** 219–225 (2000).
20. Chenn, A., Zhang, Y. A., Chang, B. T. & McConnell, S. K. Intrinsic polarity of mammalian neuroepithelial cells. *Mol. Cell. Neurosci.* **11,** 183–193 (1998).
21. Letinic, K., Zoncu, R. & Rakic, P. Origin of GABAergic neurons in the human neocortex. *Nature* **417,** 645–649 (2002).
22. Englund, C. *et al.* Pax6, Tbr2, and Tbr1 are expressed sequentially by radial glia, intermediate progenitor cells, and postmitotic neurons in developing neocortex. *J. Neurosci.* **25,** 247–251 (2005).
23. Kowalczyk, T. *et al.* Intermediate neuronal progenitors (basal progenitors) produce pyramidal-projection neurons for all layers of cerebral cortex. *Cereb. Cortex* **19,** 2439–2450 (2009).
24. Sessa, A., Mao, C. A., Hadjantonakis, A. K., Klein, W. H. & Broccoli, V. TBR2 directs conversion of radial glia into basal precursors and guides neuronal amplification by indirect neurogenesis in the developing neocortex. *Neuron* **60,** 56–69 (2008).
25. Petanjek, Z., Berger, B. & Esclapez, M. Origins of cortical GABAergic neurons in the cynomolgus monkey. *Cereb. Cortex* **19,** 249–262 (2009).
26. Götz, M. & Huttner, W. B. The cell biology of neurogenesis. *Nature Rev. Mol. Cell Biol.* **6,** 777–788 (2005).
27. Gaiano, N., Nye, J. S. & Fishell, G. Radial glial identity is promoted by Notch1 signaling in the murine forebrain. *Neuron* **26,** 395–404 (2000).
28. Shimojo, H., Ohtsuka, T. & Kageyama, R. Oscillations in Notch signaling regulate maintenance of neural progenitors. *Neuron* **58,** 52–64 (2008).
29. Abdel-Mannan, O., Cheung, A. F. & Molnar, Z. Evolution of cortical neurogenesis. *Brain Res. Bull.* **75,** 398–404 (2008).
30. Rakic, P. & Sidman, R. L. Supravital DNA synthesis in the developing human and mouse brain. *J. Neuropathol. Exp. Neurol.* **27,** 240–276 (1968).
31. Choi, B. H. Glial fibrillary acidic protein in radial glia of early human fetal cerebrum: a light and electron microscopic immunoperoxidase study. *J. Neuropathol. Exp. Neurol.* **45,** 408–418 (1986).
32. Schmechel, D. E. & Rakic, P. Arrested proliferation of radial glial cells during midgestation in rhesus monkey. *Nature* **277,** 303–305 (1979).
33. Schmechel, D. E. & Rakic, P. A Golgi study of radial glial cells in developing monkey telencephalon: morphogenesis and transformation into astrocytes. *Anat. Embryol. (Berl.)* **156,** 115–152 (1979).
34. Kriegstein, A., Noctor, S. & Martinez-Cerdeno, V. Patterns of neural stem and progenitor cell division may underlie evolutionary cortical expansion. *Nature Rev. Neurosci.* **7,** 883–890 (2006).
35. Baek, J. H., Hatakeyama, J., Sakamoto, S., Ohtsuka, T. & Kageyama, R. Persistent and high levels of Hes1 expression regulate boundary formation in the developing central nervous system. *Development* **133,** 2467–2476 (2006).

Supplementary Information is linked to the online version of the paper at www.nature.com/nature.

Acknowledgements We thank A. Alvarez-Buylla, D. Rowitch and Kriegstein laboratory members for ideas arising from discussions and for critical reading of the manuscript. We thank A. Javaherian for help setting up the conditions for dye electroporation, T. Weissman for advice on 'DiOlistics', Z. Mirzadeh for expertise with whole-mount staining, C. Harwell for retroviral production, and W. Walantus, J. Agudelo, L. Fuentealba, O. Genbacev, M. Donne and S. Kaing for other technical support. We thank R. Kageyama for his gift of the HES1 antibody[35], and F. Gage for GFP-retrovirus reagents. We thank the staff at San Francisco General Hospital for providing access to donated fetal tissue. Artwork in Fig. 5e is by K. X. Probst (Xavier Studio). This work was supported by grants from the California Institute for Regenerative Medicine and the Bernard Osher Foundation. J.H.L. is funded by a CIRM Predoctoral Fellowship.

Author Contributions D.V.H. and J.H.L. (listed alphabetically) carried out all the experiments except for the electrophysiology, analysed the data, and wrote the manuscript. P.R.L.P. performed the electrophysiology and analysed data. A.R.K., as the principal investigator, provided conceptual and technical guidance for all aspects of the project. All authors discussed the results/experiments and revised/edited the manuscript.

Author Information Reprints and permissions information is available at www.nature.com/reprints. The authors declare no competing financial interests. Correspondence and requests for materials should be addressed to A.R.K. (KriegsteinA@stemcell.ucsf.edu).

METHODS

Fetal tissue collection. Fetal cortical tissue was collected from elective pregnancy termination specimens at San Francisco General Hospital, usually within 2 h of the procedure. Tissues were examined only with previous patient consent and in strict observance of legal and institutional ethical regulations. Research protocols were approved by the Committee on Human Research (institutional review board) at University of California, San Francisco. Gestational age was determined using fetal foot length. Brain tissue was transported in L-15 medium on ice to the laboratory for further processing.

Immunohistochemistry and confocal imaging. Brain tissue was fixed in 4% PFA in PBS at 4 °C for 3 days, dehydrated in 30% sucrose in PBS, embedded and frozen at −80 °C in O.C.T. compound (Tissue-Tek), sectioned on a Leica CM3050S (50 or 20 μm) and stored at −80 °C. Cryosections were subjected to heat/citrate-based antigen retrieval for 5 min and permeabilized and blocked overnight in PBS plus 0.1% Triton X-100, 10% serum, 0.2% gelatin. Primary incubations were 3 h at room temperature or 4 °C overnight. Washes and secondary incubations were standard procedures. Vibratome-sliced sections (using Leica VT1200S at 250 or 300 μm) were not dehydrated but stained similarly except with longer antigen retrieval (15 min), antibody incubations (48 h primary, 24 h secondary at 4 °C, 0.5% Triton X-100), and washing periods. For the whole-mount stain in Supplementary Fig. 5b, the sliver ~200 μm proximal to the ventricular surface from a slab of fixed tissue was carefully microdissected and stained as if a vibratome section. Images were acquired on a Leica TCS SP5 broadband laser confocal microscope. Composite images, such as those in Fig. 4d, were automatically stitched upon acquisition using 'Tilescan' mode of Leica software. Other than Fig. 1a and Supplementary Fig. 5b, images with morphological information are maximum intensity projections collected with at least 1-μm *z*-step size. Images with nuclear staining for counting were either single optical planes or maximum intensity projections with the same number of planes and depth across compared samples. Images from Fig. 1a and Supplementary Fig. 5b were taken with a ×100 objective at 0.3-μm step size and three-dimensional-rendered using Imaris imaging software (Bitplane).

Primary antibodies were: goat anti-SOX2 (Santa Cruz sc-17320, 1:250), rabbit anti-TBR2 (Millipore AB9618 or Abcam ab23345, 1:400), mouse anti-Ki67 (Dako F7268, 1:150 for human tissue; BD Pharmingen 550609, 1:200 for mouse), rabbit anti-PAX6 (Covance PRB-278P, 1:200), mouse anti-βIII-tubulin (TuJ1, Covance MMS-435P, 1:250), rabbit anti-GABA (Sigma A2052, 1:1,000), rat anti-BrdU (Abcam ab6326, 1:100), chicken anti-GFP (Aves Labs GFP-1020, 1:1,000), mouse anti-phospho-vimentin (MBL International D076-3S (Ser 55), or D095-3 (Ser82), 1:500), rabbit anti-pericentrin (Abcam ab4448, 1:1,000), mouse anti-β-catenin (BD Transduction Labs 610153, 1:500), rabbit anti-nestin (Abcam ab5968, 1:200), rabbit anti-GFAP (Sigma G9269, 1:300), rabbit anti-DCX (Cell Signaling 4604, 1:200), rabbit anti-βIII-tubulin (Covance PRB-435P, 1:300), rabbit anti-hASH1/ASCL1 (CosmoBio SK-T01-003, 1:2,000), mouse anti-Mash1/ASCL1 (BD Pharmingen 556604, 1:500), and guinea-pig anti-HES1 (a gift from R. Kageyama[35], 1:250). Secondary antibodies were: AlexaFluor 488 (1:1,000), 546 (1:500), or 647 (1:500)-conjugated donkey anti-goat, -rabbit or -mouse IgG, or goat anti-chicken IgY (Invitrogen).

Cell counting. Confocal images (stack of ten images, 1 μm apart) were collected from sections stained for SOX2, TBR2 and Ki67. Three representative images (similar to Fig. 4d) were collected for each age. Each 'age' has $n = 1$, because recovery of usable tissue was limited. Fluorescence signal from nuclear immunoreactivity of SOX2, TBR2 and Ki67 was first counted individually using the 'spots' function in Imaris imaging software (Bitplane). A threshold for intensity mean was set to find fluorescent spots sized at 5-μm diameter from each channel as a representation of the number of actual cells. The preliminary sets of positive cells were then manually edited to correct software error. Double and triple co-localized spots were then calculated by Matlab (Mathworks) and the ImarisXT (Bitplane) module, and further edited to correct software errors. The numbers of total and co-localized spots were recorded and subtracted from each other to determine the number of single-, double- and triple-labelled cells. Counts from VZ–ISVZ and OSVZ were separated by a line defined by the outer limit of dense $TBR2^+$ staining in the ISVZ. Percentages were calculated within each sample and then averaged across the three images. OSVZ cell counts from Fig. 5a and Supplementary Figs 1 and 10 were done similarly.

Counts using oRG cell morphology as an initial measure (cells with phospho-$vimentin^+$ basal fibres, $adenoGFP^+$ cells in HES1, BrdU and EdU labelling) were done by first identifying OSVZ cells that had long basal but not apical processes, and then examining their co-localization with markers in the other channels.

Co-localization of BrdU, TBR2 and GABA with βIII-tubulin in dissociated cells was counted manually in 25 fields of vision. Centrosome occupation of RG endfeet was counted in five fields of more than 100 endfeet by first identifying clear endfeet (areas outlined by β-catenin—while blinded to pericentrin), and then subtracting the number of endfeet that did not contain pericentrin.

In the Notch-inhibition experiments, the nuclear fluorescence of SOX2 and either TBR2 or ASCL1 was calculated by first finding 5-μm diameter spheres from the DAPI channel (as a volumetric representation of the nuclei) in two fields of OSVZ cells (cell number >1,200) for each condition using Imaris Spots, and then calculating fluorescence intensity mean values in each spot volume for the other two channels. Background (the lowest recorded intensity mean for each channel) was subtracted from the paired values and then shown as scatter plots (Fig. 5d and Supplementary Fig. 14).

Dissociated cortical cell culture and immunocytochemistry. GW15.5 cortex was vibratome-sliced at 300-μm thickness. Each slice was individually microdissected into three portions (VZ–ISVZ, OSVZ and CP) based on the columnar or stratified appearance of different regions that could be visualized under the dissecting microscope. We purposely erred towards the pial surface for both cuts to avoid contamination of OSVZ with VZ–ISVZ cells, and to avoid contamination of CP with OSVZ cells. VZ–ISVZ, OSVZ and CP from seven individual slices were pooled and dissociated using papain (Worthington Biochemical Corporation) at 37 °C for 20 min and then trituration. Cells were pelleted by centrifugation, resuspended, passed through cell-strainer caps, repelleted and resuspended. Cells were plated at 120,000 cells per well on 4-well Nunclon Δ multidishes (Sigma) coated with poly-L-ornithine (Sigma) and laminin (Invitrogen) in RHB-A medium (Stem Cell Sciences) plus BrdU (Sigma, 15 μg ml^{-1}) and cultured at 37 °C, 5% CO_2 for 1 week with medium exchanged every 2 days. Cells were fixed in 4% PFA for 20 min and processed for immunofluorescence microscopy as described earlier with some exceptions. GABA stains were performed before antigen retrieval and in the absence of detergent, followed by another PFA fixation, antigen retrieval and normal staining for other antigens. For BrdU detection, all other antigens were stained first and fixed with PFA, followed by 20 min in 2 N HCl, several rinses with buffer, and finally BrdU immunostaining.

Dye electroporation. Lysine-fixable TexasRed-dextran (Molecular Probes) was focally electroporated into the OSVZ of 250-μm vibratome slices from GW15.5 cortex (for Fig. 1a) and GW14 (Supplementary Fig. 2) using similar methods as previously described[15]. A P-97 micropipette puller (Sutter) was used to generate pipettes of 0.6–1.0-μm tip width. Electrical stimulation was generated by the Grass S48 Stimulator (5 pulses per second for 1 second at a time, pulse duration of 2 ms, voltage of 30–100 V). Dye was allowed to diffuse for 30 min before fixation and immunostaining.

DiOlistics labelling. GW15 cortical slabs were fixed in 4% PFA in PBS for 24 h. After soaking the fixed tissue overnight in PBS plus 0.4% EDTA, we used the published 'DiOlistics' gene gun protocol[19] to apply DiI-coated beads to either the pial or ventricular surface, with the following modifications: 1.1-μm tungsten microcarriers (Bio-Rad) were coated with fixable CellTracker CM-DiI (Molecular Probes). The Bio-Rad Helios Gene Gun System was substituted with a common air duster (Fellowes). The beads were shot through 3.0-μm pore size filters from Transwell Permeable Supports (Costar). CM-DiI was allowed to diffuse throughout the tissue in 0.4% EDTA in PBS for 3.5 weeks and then fixed in 4% PFA and vibratome-sliced for imaging analysis.

Viral infection, cortical slice culture and real-time imaging. For Fig. 1b, replication-incompetent enhanced-GFP-expressing retrovirus (1×10^6 colony forming units (c.f.u.)) was applied to a cortical slab for 1 h at room temperature in a minimal volume of artificial cerebrospinal fluid (ACSF; 125 mM NaCl, 2.5 mM KCl, 1 mM $MgCl_2$, 2 mM $CaCl_2$, 1.25 mM NaH_2PO_4, 25 mM $NaHCO_3$, 25 mM D-(+)-glucose, bubbled with 95% O_2/5% CO_2). Tissue was then embedded in 4% low melting point agarose in ACSF, and vibratome-sliced at 250 μm in ice-chilled ACSF. Slices were transferred to and suspended on Millicell-CM slice culture inserts (Millipore) over culture medium in culture well plates and incubated at 37 °C, 5% CO_2.

For all time-lapse imaging, as well as the BrdU, EdU and Notch experiments, 250–300-μm vibratome slices were generated and suspended in culture medium as described earlier, and CMV-GFP adenovirus (Vector Biolabs, 1×10^6 c.f.u.) was injected focally into the cortical plate all along the slice to achieve sparse labelling in the OSVZ. Slices were first cultured at 37 °C, 5% CO_2, 8% O_2 for ~24 h. Cultures were then transferred to an inverted Leica TCS SP5 with an on-stage incubator (while streaming 5% CO_2, 5% O_2, balance N_2 into the chamber), and imaged using a ×40 air objective at 20–22-min intervals (as specified) for up to 6 days with intermittent repositioning of the focal planes. Maximum intensity projections of the collected stacks (~30 μm at ~2.5-μm step size) were compiled and generated into movies. Mitotic somal translocation distances were measured using Imaris. Only mitotic cells that had long basal processes and no apical ones were considered as oRG cells.

All slice cultures other than those in Fig. 5 were cultured in 66% BME, 25% Hanks, 5% FBS, 1% N-2, 1% penicillin, streptomycin and glutamine (all

Invitrogen) and 0.66% D-(+)-glucose (Sigma). For Fig. 2a, BrdU (Sigma, 15 μg ml^{-1}) was added at the beginning of slice culture and washed out after 12 h. EdU (Invitrogen, 15 μg ml^{-1}) was added 36 h after the initial pulse of BrdU and then fixed 48 h later. Slices were stained using EdU Click-iT (Invitrogen) and standard procedures. For Fig. 5d and Supplementary Fig. 14, slices were cultured in RHB-A medium plus 10 μM DAPT (Biomol International) or DMSO (control).

Electrophysiology. GW15 (time-lapse slices) and GW17 (blind acute recordings) cortical slices were prepared as earlier, or after time-lapse imaging, and held in room temperature ACSF until being moved to a 32 °C submersion-type chamber for recordings. Cells were targeted for recording by differential interference contrast (DIC) imaging or GFP immunofluorescence in slices that were previously time-lapse imaged. Patch pipettes were made from 1.5-mm outer diameter (OD)/0.86-mm inner diameter (ID) glass (Corning) and filled with (in mM) 130 K-gluconate, 4 KCl, 2 NaCl, 10 HEPES, 0.2 EGTA, 4 ATP-Mg, 0.3 GTP-disodium, 14 phosphocreatine-dipotassium (pH 7.25, 280–290 mOsm). For morphological reconstruction, 50 μM TexasRed-dextran (Molecular Probes) was included in the recording solution. Tetrodotoxin (TTX, 0.5 μM, Calbiochem) was perfused onto cells locally using an Octaflow drug application system (ALA Scientific Instruments). Series resistances were typically between 5 and 15 MΩ and were continually monitored and compensated for throughout the recording sessions. Recordings were performed with a MultiClamp 700B amplifier (Axon Instruments) under infrared-differential interference contrast visualization using an Olympus BX50WI and a CCD camera (MTI). Recordings were acquired and analysed using pClamp version 10 (Axon Instruments) and data were further analysed in Excel (Microsoft). Input resistance was calculated from small (3–5 mV) 600-ms voltage deflections induced by square hyperpolarizing current injections (averages of 20–40 deflections) in current clamp. Sodium currents were measured in voltage clamp. All averages reported are mean ± standard error.